Segmented Replicated X-Ray Optics: A concept for future flagship X-ray telescope

Panini S. Singam[a,b], David D.Smith[b], Jessica A. Gaskin[b], Stephen D. Bongiorno[b], Danielle N. Gurgew[a,b], David A. Banks[b], Amy B. Meekham[c,b], Julian Torstenson[d], Nicholas E. Thomas[b], Walter P. Maksym[b], Kirtan P. Dixit[e,b], and Brian D. Ramsey[b]

[a]Universities Space Research Association, Huntsville, Alabama, USA
[b]NASA Marshall Space Flight Center, Huntsville, Alabama, USA
[c]Amentum, Huntsville, Alabama, USA
[d]New Century Technology High School, Huntsville, Alabama, USA
[e]Oak Ridge Associated Universities, Oak Ridge, Tennessee, USA

ABSTRACT

Next-generation X-ray observatories like the Lynx X-ray Observatory require unprecedented collecting areas approaching 2 m^2 with sub-arcsecond angular resolution. This necessitates mirror shells with diameters reaching 3 meters. Conventional full-shell replicated X-ray optics present substantial cost and technical challenges at these scales. Meter-scale optics introduce significant handling complexity despite simplified assembly procedures. The X-ray Optics group at NASA Marshall Space Flight Center (MSFC) is investigating Segmented Replicated X-Ray Optics (SRXO) as an alternative approach. This concept leverages MSFC's established electroforming replication capabilities refined over three decades. The segmented architecture exploits the azimuthal symmetry of Wolter-type geometries. Multiple shell segments can be replicated from single segmented mandrels, substantially reducing mandrel fabrication costs. Unlike conventional full shells, SRXO can maintain smaller mirror thickness for large diameter shells. This yields significant mass reductions and facilitates improved quality control. This paper introduces the SRXO concept and presents initial results from our feasibility study. We present metrology of fabricated segments along with modeling results to understand the underlying physical processes. These preliminary findings demonstrate the potential viability of the segmented approach for meeting next-generation observatory requirements.

Keywords: X-ray optics, Electroforming, Segmented X-ray optics

1. INTRODUCTION

The X-ray Optics group at NASA Marshall Space Flight Center (MSFC) has developed and refined electroforming replication technology for X-ray optics fabrication over more than three decades. This process involves precision polishing of cylindrical mandrels to excellent figure accuracy, followed by electroforming nickel shells that replicate the mandrel surface. The electroformed shells are then separated from the mandrel to create lightweight, high-resolution X-ray mirrors.[1–3] Full shell geometry offers several distinct advantages: structurally stable geometry that maintains the optical figure under various loading conditions, reduced alignment errors during telescope assembly, excellent endurance under coating and deposition stresses, and compatibility with multiple module designs for the effective scaling area.[4,5] MSFC's approach benefits from high-resolution mandrel polishing capabilities, excellent control over the replication process, and extensive flight heritage including balloon-borne telescopes (HERO),[6] sounding rocket payloads (FOXSI),[7–9] and satellite missions such as the Imaging X-ray Polarimetry Explorer (IXPE).[10]

Alternative approaches to X-ray optics fabrication employ segmented mirror technologies, where the telescope aperture is divided into numerous precisely fabricated and polished segments that collectively form the complete optical system. In this concept, individual mirror segments are manufactured to high precision and then carefully

Further author information: (Send correspondence to P.S.)
P.S.: E-mail: srikanthpanini.singam@nasa.gov

assembled into nested shell configurations following Wolter I geometry. This segmented approach allows for distributed manufacturing and improved quality control at the segment level. Two prominent examples of segmented X-ray optics include Silicon meta-shell optics developed at NASA Goddard Space Flight Center[11] and slumped glass technologies used for the NuSTAR observatory.[12] Silicon meta-shells utilize precisely machined silicon wafers with deterministic surfaces that are stacked and bonded to create nested shell segments. The silicon approach offers exceptional surface quality, dimensional stability, and the potential for automated assembly processes. Slumped glass techniques involve thermally forming thin glass substrates over precision mandrels to create lightweight mirror segments with smooth surfaces. Both approaches provide advantages in segment-level quality control, scalability to large collecting areas. However, segmented mirror systems require more complex assembly procedures compared to full shell configurations. The mounting and alignment of multiple segments necessitates sophisticated metrology and precision positioning systems to achieve sub-arcsecond X-ray imaging performance.

The proposed Lynx X-ray Observatory represents a significant advancement in X-ray astronomy capabilities, requiring an effective area of approximately 2 m^2 at 1 keV with sub-arcsecond imaging resolution.[13] Additionally, Lynx demands high spectral resolution ($\Delta E/E > 3000$) to enable detailed spectroscopic studies of cosmic phenomena. Meeting these spectral requirements necessitates the use of microcalorimeter detectors, which operate at millikelvin temperatures and require sophisticated cryogenic systems. The complexity and cost of these detector systems make it impractical to implement the traditional MSFC approach of multiple identical telescope modules, each with its own focal plane instrument. Our approach to produce multiple modules by reusing the super polished mandrels greatly increases the efficiency of the fabrication process. However, achieving Lynx-level effective area would require mirror shells with diameters up to 3 meters, presenting substantial structural challenges for monolithic full shells. The large size introduces significant handling difficulties, increased susceptibility to deformation under loads, and potential degradation of imaging performance due to structural instabilities.

To address these challenges, while leveraging MSFC's extensive experience in mandrel polishing and electroforming, we are investigating Segmented Replicated X-ray Optics (SRXO) technique. This approach modifies the geometry from full cylindrical mandrels to segmented mandrel surfaces, allowing us to apply our proven fabrication heritage to a new architectural concept. By segmenting the mandrel geometry, we can maintain the benefits of our established electroforming process while addressing the scalability and structural challenges associated with very large diameter optics.

2. SEGMENTED REPLICATED X-RAY OPTICS

Segmented Replicated X-ray Optics (SRXO) addresses the fundamental challenges faced by full-shell X-ray optics at large scales while preserving the benefits of MSFC's proven electroforming technology. The SRXO approach utilizes mandrels that are inherently segmented in geometry, representing angular portions of what would otherwise be complete cylindrical mandrels. Multiple identical segments are replicated from a single segmented mandrel and then assembled to construct the complete cylindrical X-ray optic. This strategy directly addresses the most expensive and time-consuming aspect of replication technology: mandrel fabrication and polishing to sub-arcsecond figure and roughness accuracies.

The segmented approach offers substantial improvements in production efficiency and cost reduction. Traditional full-shell fabrication requires manufacturing and polishing complete cylindrical mandrels, which becomes increasingly challenging and expensive as diameters scale to meter-class dimensions. With SRXO, a single segmented mandrel can produce multiple identical segments, dramatically improving cost-effectiveness by amortizing the mandrel fabrication investment across numerous replicated parts. The segmented mandrels are significantly easier to handle, machine, and polish compared to their full-scale cylindrical counterparts at large diameters, while maintaining the same axial length and optical prescription accuracy. This approach provides a unique advantage over other segmented mirror technologies, such as Silicon meta-shells, where each individual segment must be independently polished and figured to the required specifications. In contrast, SRXO leverages the replication process to transfer the surface quality from a single super-polished mandrel to multiple segments, eliminating the need for individual segment polishing. Even if future sub-arcsecond requirements necessitate additional super-polishing at the segment level, the replicated segments begin with surface qualities inherited from

the precision mandrel, requiring only minimal material removal for final figuring rather than complete surface development from raw substrates.

Scalability to larger diameters represents another significant advantage of the segmented approach. Individual segments derive their structural stability from the mounting system rather than relying on shell thickness for rigidity. This eliminates the need to fabricate massive 3-meter diameter mandrels or handle the resulting heavy replicated shells. For example, a single 3-meter NiCo shell with 1 mm thickness and 60 cm length (combining parabolic and hyperbolic sections) would weigh approximately 50 kg. Full shells require increased thickness with diameter to maintain structural stability, further increasing mass and handling complexity. The segmented architecture avoids these scaling issues entirely, as individual segments maintain consistent dimensions regardless of the final telescope diameter.

The SRXO fabrication process closely parallels the established full-shell replication methodology, leveraging MSFC's decades of experience with minimal process modifications. The process begins with segmented aluminum mandrels (Figure 1a) that represent angular portions of the complete Wolter geometry. Similar to full-shell fabrication, the aluminum substrate is coated with electroless nickel-phosphorus (NiP), diamond-turned to achieve the desired figure, and then precision-polished to the required surface roughness. The segments are then electroformed in an optimized bath geometry (Figure 1b) using the same nickel-cobalt alloy employed in full-shell production. The electroforming parameters, including current density, bath chemistry, and deposition stress control, remain consistent with proven full-shell processes, ensuring that the accumulated expertise directly transfers to the segmented approach.

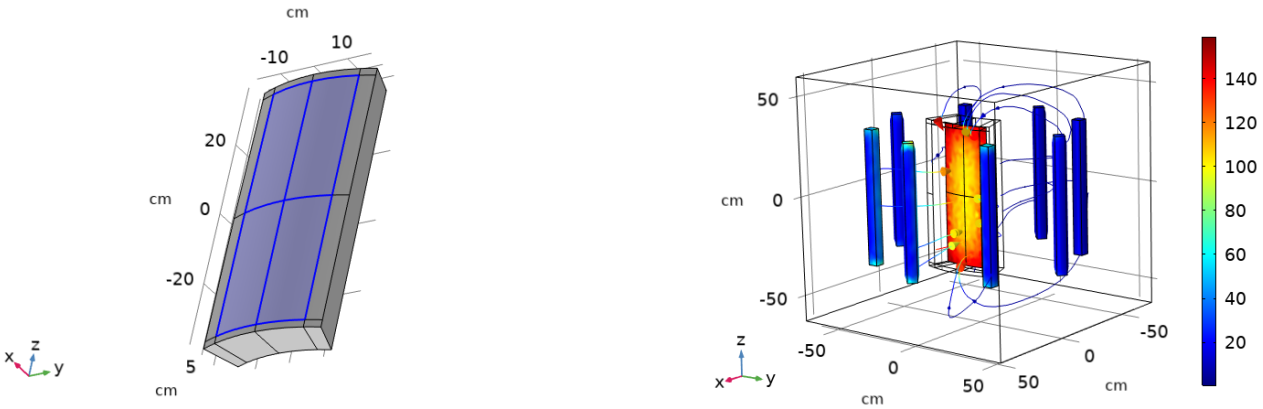

(a) (b)

Figure 1: SRXO fabrication process: (a) Segmented mandrel geometry representing an angular portion of the complete Wolter optic, and (b) electroforming setup with optimized bath configuration for segment replication. The color bar represents the change in thickness in μm

3. PROTOTYPE SRXO FABRICATION

To understand the fabrication process and identify key aspects of SRXO production, we have fabricated prototype segments using our established electroforming process with modifications to accommodate segmented geometries. For this initial feasibility study, we utilized an existing full-shell mandrel rather than fabricating dedicated segmented mandrels. During the replication process, insulating tape was strategically applied to define the boundaries of individual segments on the mandrel surface. This approach enabled the simultaneous fabrication of multiple segments with varying axial lengths and azimuthal extents from a single mandrel in one electroforming run, providing valuable insights into the segmented replication process.

The prototype fabrication process begins with boundary definition on the cylindrical mandrel using insulating tape (Figure 2a). The tape serves as a mask, preventing electroforming in designated areas and creating discrete segment regions. Following boundary establishment, the mandrel undergoes passivation treatment with

potassium dichromate solution (Figure 2b). This chemical passivation process creates a thin oxide layer on the mandrel surface that facilitates clean separation of the electroformed segments after deposition while maintaining the surface quality transfer from mandrel to shell. The electroforming process proceeds using our standard nickel-cobalt (NiCo) alloy chemistry, with segments growing simultaneously across the defined regions (Figure 2c). The deposition continues until the desired thickness of approximately 350 μm is achieved, consistent with our full-shell fabrication parameters.

The electroformed mandrel assembly is immersed in ice water (Figure 3a), causing differential thermal contraction between the aluminum mandrel and NiCo segments due to their mismatched coefficients of thermal expansion. This differential contraction overcomes the electroforming adhesion forces, enabling clean segment release from the mandrel surface (Figure 3b). The process yields multiple discrete segments (Figure 3c) that maintain the optical surface quality of the original mandrel while providing the geometric flexibility required for segmented telescope architectures.

(a) (b) (c)

Figure 2: Prototype SRXO setup and electroforming: (a) cylindrical mandrel with insulating tape boundaries defining segment regions, (b) potassium dichromate passivation treatment for enhanced shell release, and (c) electroformed mandrel with 350-micrometer NiCo segments.

4. AXIAL PROFILE MEASUREMENT

We employed Zygo interferometry to measure the axial figure distortion of the fabricated segments, providing quantitative assessment of the optical quality transferred from the mandrel to the replicated segments. Axial profile measurements are extremely sensitive to segment alignment during metrology, as misalignment introduces systematic errors that can obscure the true optical figure. In particular, tilt errors cause contamination of the axial curvature measurements with the dominant azimuthal curvature of the Wolter geometry, leading to erroneous figure assessments. To address these alignment challenges, we developed a specialized metrology setup that suspends the segment at two precisely controlled points using pico-actuators for fine tilt adjustments (Figure 4). The segment is mechanically stabilized using a three-point kinematic mount to minimize vibrations and maintain stable positioning during measurements. This configuration allows for precise alignment of the segment axis with the interferometer measurement beam while providing the mechanical stability necessary for high-precision figure measurements. The pico-motor suspension system enables sub-micrometer positioning control, ensuring that the segment can be accurately oriented relative to the interferometer reference beam.

(a) (b) (c)

Figure 3: Prototype SRXO separation process: (a) thermal separation process using ice water immersion, (b) segment release from mandrel due to differential thermal contraction, and (c) collection of fabricated segments with varying geometries.

The measured axial profiles for both parabolic and hyperbolic segments are presented in Figure 5, with the theoretical Wolter prescriptions subtracted to reveal figure errors. The hyperbolic segment (Figure 5a) exhibits a an axial profile with peak-to-valley deviations of approximately 18 microns over the axial length. The parabolic segment (Figure 5b) shows similar behavior with about 13 microns deviations near the segment boundaries. Both profiles demonstrate dominant low-frequency axial curvature errors that deviate from the ideal Wolter prescription. These measurements indicate that the segments retain figure distortions that may originate non-uniform electroforming stresses. The observed local curvature variations in the axial direction suggest systematic deviations from the ideal optical prescription that will require further investigation and process optimization to achieve sub-arcsecond imaging performance.

5. MODELING OF ELECTROFORMING STRESS EFFECTS

To investigate the possible origin of the observed curvature errors in the fabricated segments, we developed finite element models to analyze the effects of residual electroforming stress on segment geometry. In our previous work on full-shell optics, we demonstrated that electroforming stresses primarily affect the edge regions of the shell shells, with minimal impact on the central optical regions and consequently limited degradation of half-power diameter (HPD) performance. We applied a similar modeling framework to understand stress effects in the segmented geometry, recognizing that the altered boundary conditions and reduced structural constraints of segments may lead to different stress response characteristics.

Our finite element analysis reveals that uniform electroforming stress across the segment surface does not introduce significant curvature distortions. Figure 6 demonstrates this behavior for both compressive and tensile stress conditions. The uniform compressive stress case (Figure 6a) and uniform tensile stress (Figure 6b) produces low-level response without introducing systematic curvature errors. These results indicate that homogeneous electroforming conditions would not be expected to produce the observed axial figure distortions. However, when spatially varying stress distributions are introduced across the segment surface, the modeling reveals significant curvature generation (Figure 6c). Non-uniform stress patterns, which can arise from variations in current density during electroforming, electric field non-uniformities, produce deformation patterns that closely resemble the measured axial figure errors. The magnitude and spatial distribution of these stress-induced deformations are consistent with the observed curvature characteristics in our prototype segments. These findings strongly suggest

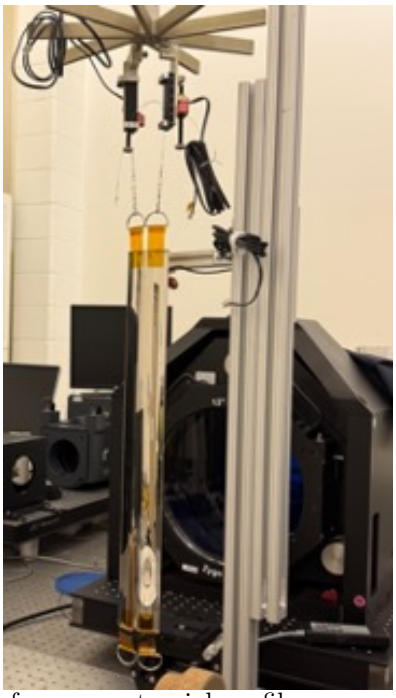

Figure 4: Specialized metrology setup for segment axial profile measurement using Zygo interferometry. The segment is suspended at two points using pico-actuators for precise positioning control and stabilized with a three-point kinematic mount to minimize vibrations during measurements.

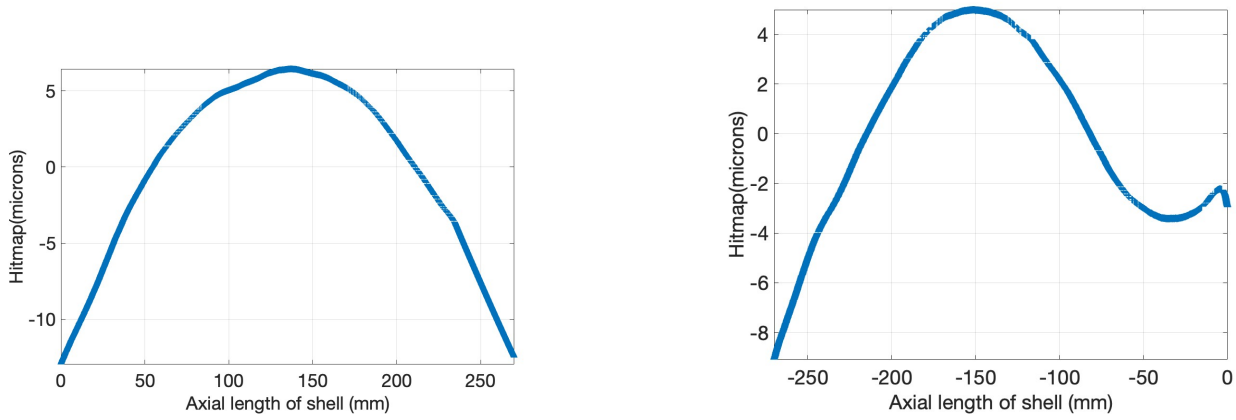

(a) (b)

Figure 5: Axial profile measurements of prototype segments with prescription subtracted. Measurements are taken close to the center of the segment: (a) hyperbolic segment showing peak-to-valley deviations of approximately 18 μm over axial length, and (b) parabolic segment exhibiting similar low-frequency figure errors with peak-to-valley variations of approximately 12 μm over axial length.

that the dominant curvature errors observed in our segments originate from non-uniform electroforming stress distributions rather than systematic mandrel errors or thermal effects during separation.

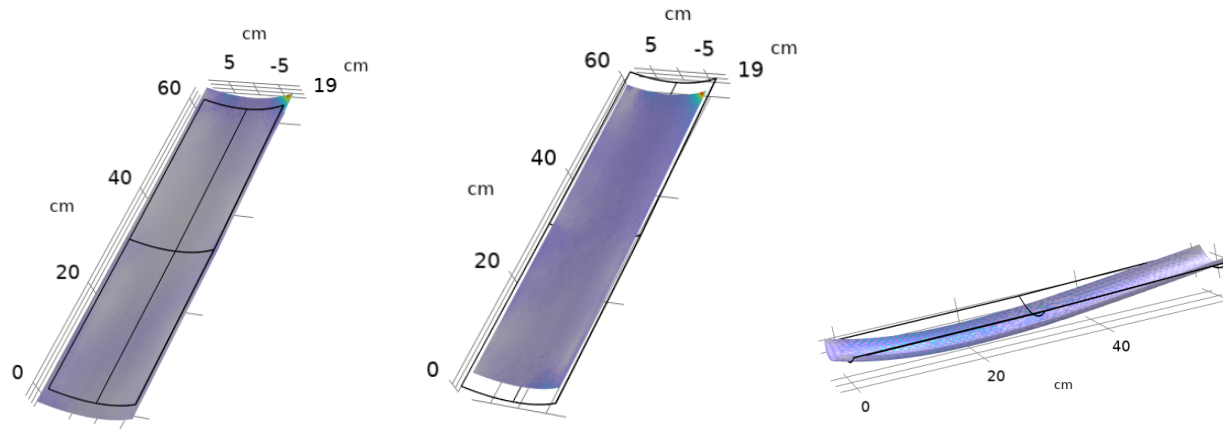

(a) (b) (c)

Figure 6: Finite element modeling of electroforming stress effects on segment geometry (solid lines represent the dimensions of the segment boundaries before deformation): (a) A representative uniform compressive stress. (b) uniform tensile stress exhibiting similar low-level response without systematic curvature, and (c) spatially varying stress (inverted-gaussian shape with minimum stress in the center and maximum at the edges) distribution producing significant curvature distortions consistent with measured segment figure errors.

6. THICKNESS UNIFORMITY MEASUREMENT

In electroforming processes, the deposition rate is directly proportional to the local current density at the cathode surface, which in turn directly influences the local stress fields within the deposited material. By measuring the thickness uniformity of fabricated segments, we can obtain quantitative estimates of stress variations across the surface that may be responsible for the observed curvature distortions. This relationship between current density, deposition rate, and residual stress provides a pathway for understanding and potentially controlling the figure errors observed in our prototype segments.

We employed ultrasonic thickness measurements to characterize the spatial distribution of thickness variation across the segment surface. Multiple measurement points were taken across both the axial and azimuthal dimensions of the segment to provide comprehensive coverage of the optical surface. Figure 7 presents the measured thickness profile with circular markers indicating the discrete measurement locations and color coding representing the interpolated thickness variation across the entire segment surface. Thickness measurements are not performed at the edges of the segments. Hence it misses out the large thickness regions at the edges.

The thickness measurements clearly demonstrate significant non-uniformity across the segment, with the material being substantially thicker at the edge regions compared to the central areas. The thickness variation ranges from approximately 400 μm in the central regions to over 560 μm near the segment boundaries, representing a variation of more than 35% across the surface. This edge thickening behavior is consistent with observations in our full-shell fabrication processes, where sharp discontinuities in the cathode geometry concentrate the local electric field at boundaries, leading to enhanced current density and accelerated deposition rates.

The pronounced thickness non-uniformity directly correlates with the spatial stress variations. The regions of excessive thickness deposition correspond to areas of elevated electroforming stress, which subsequently manifest as the curvature distortions observed in our axial profile measurements. This finding confirms that controlling the electric field distribution during electroforming will be critical for achieving the uniform deposition necessary for high-quality segmented optics. The thickness measurement results provide clear evidence that the dominant curvature errors in our prototype segments originate from non-uniform electroforming conditions rather than mandrel figure errors or separation-induced distortions.

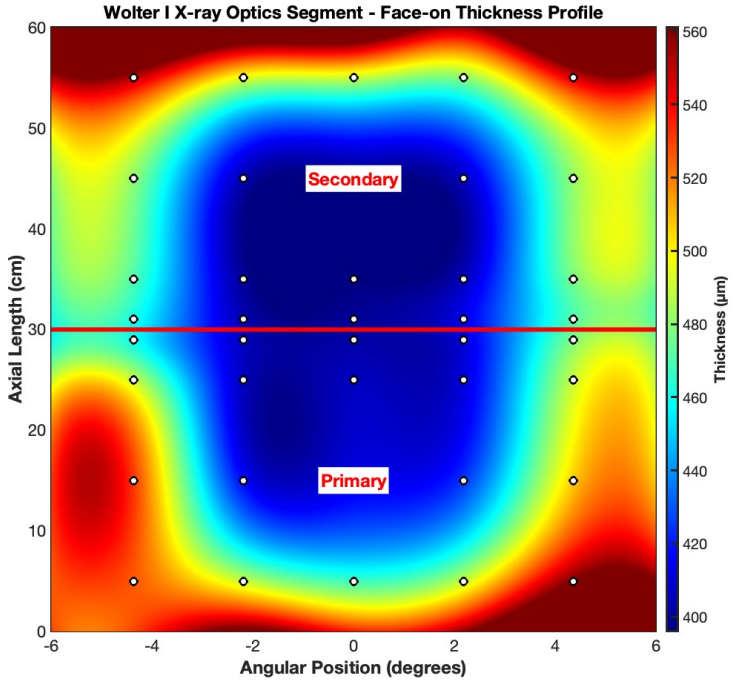

Figure 7: Measured thickness profile of prototype segment using ultrasonic measurements. Circular markers indicate measurement locations with color coding representing interpolated thickness variations across the surface. The data reveals significant non-uniformity with thickness ranging from 400 μm in central regions to over 560 μm at the edges, indicating substantial current density variations during electroforming.

7. OPTIMIZING THICKNESS UNIFORMITY

Building upon our established techniques for full-shell electroforming optimization, we have investigated several approaches to improve electric field distribution and thickness uniformity for segmented geometries. The fundamental principles developed for full-shell optics can be adapted to address the unique boundary conditions present in segmented mandrels, where sharp discontinuities at segment edges create localized field concentrations that lead to non-uniform deposition.[14,15]

We use insulating gaskets at segment boundaries to define the electroforming regions and control local electric field distributions. The baseline configuration uses gaskets with minimal height above the mandrel surface (Figure 8a), resulting in significant thickness non-uniformity with pronounced edge thickening (Figure 8b). These results are obtained from finite element modelling in COMSOL. The thickness profile shows large variations between central and edge regions, with the characteristic sharp increases at segment boundaries due to electric field concentration.

Increasing the gasket height substantially above the mandrel surface provides significant improvement in thickness uniformity (Figure 9a). The elevated gaskets act as field-shaping elements that redistribute the electric field lines away from the segment edges, resulting in a uniform current density across the optical surface. The corresponding thickness profile (Figure 9b) demonstrates dramatically improved uniformity, with variations reduced to approximately 50 μm across the segment width. This technique effectively extends the controlled deposition region while minimizing edge effects that dominate the baseline configuration.

However, large gasket heights introduce practical complications during electroforming. The elevated structures create regions of restricted electrolyte flow and can generate turbulent mixing when the mandrel rotates about its axis during deposition. These flow disturbances can lead to localized chemistry variations and introduce new sources of thickness non-uniformity, particularly in long-duration electroforming runs where electrolyte circulation becomes critical for maintaining stable deposition conditions.

An alternative approach involves strategically placing copper tape on the gasket surfaces and connecting them electrically to the cathode circuit. This configuration allows controlled electroforming on the gasket regions themselves, effectively making the gaskets part of the active deposition surface (Figure 10a). The copper tape placement at all four corners of the segmented mandrel creates a more uniform current density distribution at the segment boundaries by providing additional current paths that reduce field concentration at the optical surface edges. Finite element simulation in COMSOL of this tape-enhanced configuration (Figure 10b) shows substantial improvement in azimuthal thickness uniformity, with the sharp edge peaks eliminated and overall thickness variation reduced to less than 100 μm across the segment. This approach maintains the benefits of improved thickness uniformity while avoiding the electrolyte flow complications associated with large gasket heights.

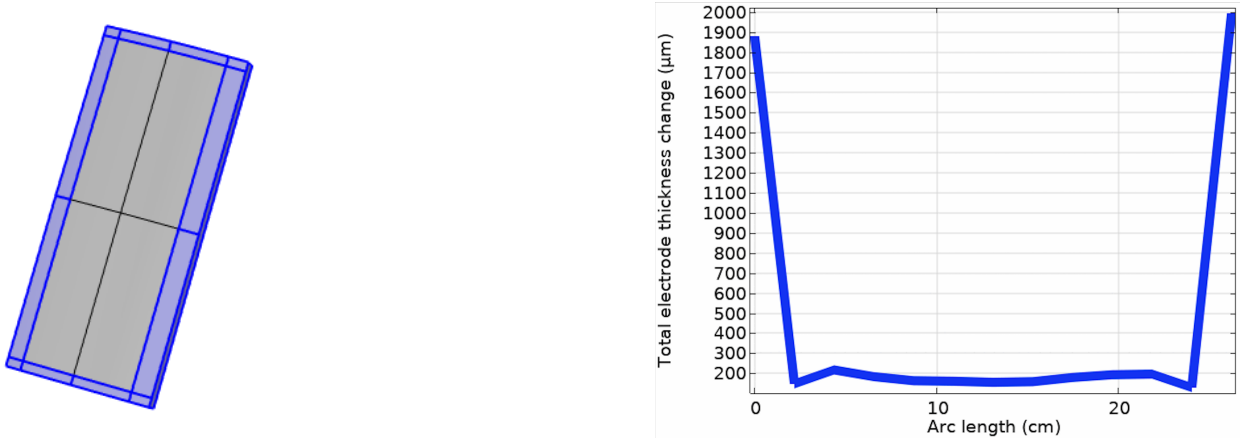

(a) (b)

Figure 8: Baseline gasket configuration: (a) segmented mandrel with minimal gasket height, and (b) resulting thickness profile along the azimuthal direction showing severe non-uniformity with thickness variations exceeding 1500 μm at segment boundaries.

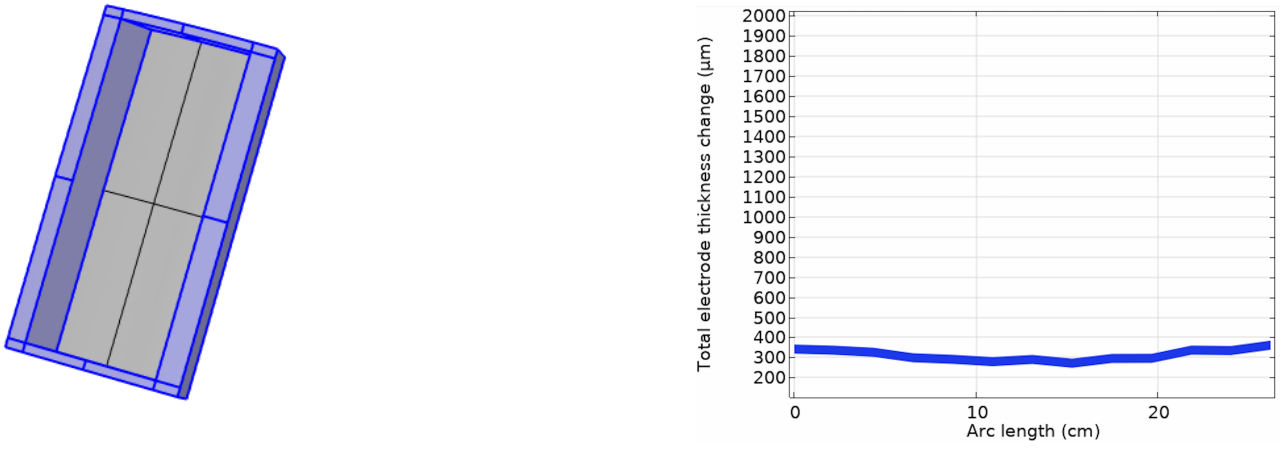

(a) (b)

Figure 9: Large gasket height configuration: (a) segmented mandrel with elevated gaskets for field shaping, and (b) significantly improved thickness uniformity with variations reduced to approximately 50 μm along the azimuthal direction of the segment.

These electric field optimization techniques directly address the major root cause of figure distortions observed

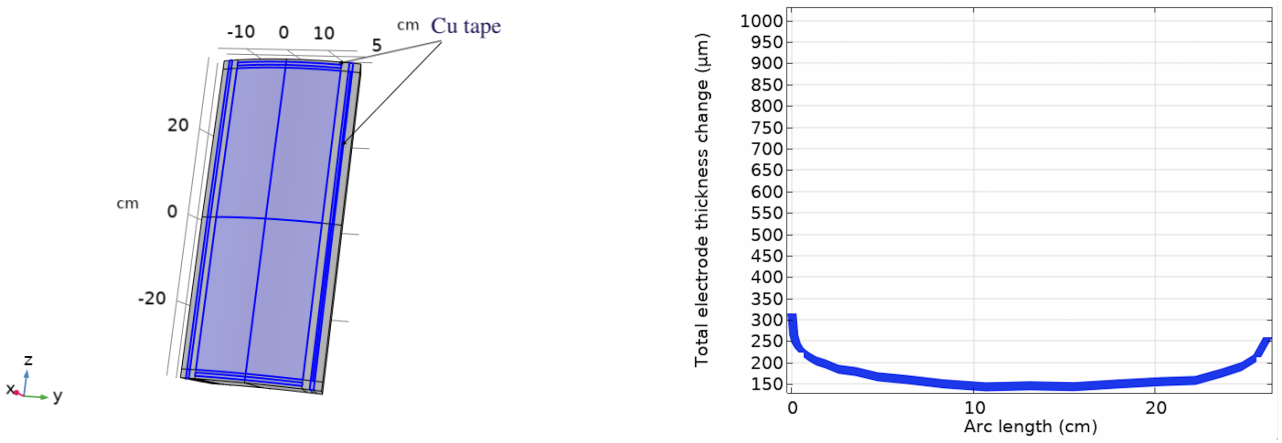

(a) (b)

Figure 10: Copper tape optimization method: (a) schematic showing copper tape placement on gasket corners connected to cathode circuit, and (b) simulated azimuthal thickness profile demonstrating improved uniformity with edge peak elimination and overall variation reduced to less than 100 μm.

in our prototype segments. By achieving uniform thickness deposition, we create correspondingly uniform stress distributions that minimize the curvature-inducing effects identified through our modeling and measurements. The application of these proven full-shell optimization methods to segmented geometries provides a clear pathway for dramatically improving segment optical quality. As demonstrated in our full-shell work, systematic electric field control can reduce thickness variations, which translates directly to improved figure quality and enhanced imaging performance for the segmented architecture.

8. SUMMARY AND FUTURE WORK

This paper introduces Segmented Replicated X-ray Optics (SRXO) as a promising approach to address the scalability challenges faced by conventional full-shell X-ray optics for next-generation observatories like Lynx. The SRXO concept leverages MSFC's proven electroforming replication technology while utilizing segmented mandrel geometries to enable cost-effective production of large-diameter telescope systems. Our prototype fabrication demonstrates the feasibility of the segmented approach, successfully producing multiple segments from a single mandrel using modified full-shell processes. Metrology of the fabricated segments reveals figure distortions that correlate strongly with non-uniform thickness deposition, which our modeling attributes to spatially varying electroforming stresses caused by electric field concentrations at segment boundaries. The observed thickness variations, ranging from 400 to over 560 μm across segment surfaces, directly translate to the curvature errors measured in axial profile characterization. Our investigation of electric field optimization techniques, including gasket height adjustment and copper tape placement, demonstrates clear pathways for achieving the uniform deposition necessary for high-quality segmented optics.

Future work will focus on implementing optimized electric field control techniques in dedicated segmented mandrel fabrication to validate the effectiveness of these approaches in actual segment production. We will continue developing prototype segments using proven optimization methods to demonstrate improved figure quality that matches mandrel prescriptions within the tolerances required for sub-arcsecond imaging performance. We are also investigating the effects of coating-induced stresses on segmented optics performance. Our previous analysis of thin film and multilayer coating stresses in full-shell configurations demonstrated the inherent stability of full shells to these deposition-induced effects.[16] However, segmented geometries exhibit greater susceptibility to coating stresses due to reduced structural constraints and altered boundary conditions.[17] To address this challenge, we are developing stress-reduced coating techniques and optimized deposition parameters that minimize figure distortions while maintaining the reflectivity and broadband spectral performance required for X-ray applications. In parallel, we are working on building an automated metrology system capable of rapid, high-precision measurement of both axial and azimuthal profiles for comprehensive segment characterization. Additionally, we

plan to optimize mandrel polishing techniques specifically for segmented geometries, adapting our established full-shell polishing processes to the unique requirements of angular mandrel sections. These combined efforts will establish SRXO as a viable technology for meeting the demanding requirements of future flagship X-ray missions while leveraging the extensive heritage and proven capabilities of MSFC's electroforming replication program.

REFERENCES

[1] Ramsey, B. D., "Replicated nickel optics for the hard-x-ray region," *Experimental astronomy* **20**(1-3), 85–92 (2005).

[2] Kilaru, K., Ramsey, B. D., Bongiorno, S. D., Kolodziejczak, J. J., O'Dell, S. L., Weisskopf, M. C., Elsner, R. F., Gubarev, M. V., McClelland, R., Gaskin, J. A., et al., "Full-shell x-ray optics development at nasa marshall space flight center," *Journal of Astronomical Telescopes, Instruments, and Systems* **5**(2), 021010 (2019).

[3] Champey, P. R., Smith, D. D., Singam, P., Bongiorno, S. D., Gaskin, J. A., and Ramsey, B. D., "Toward the fabrication of a 5 micron-resolution wolter microscope for the national ignition facility," *Review of Scientific Instruments* **93**(11), 113504 (2022).

[4] Kolodziejczak, J., Gaskin, J., Baumgartner, W., Bongiorno, S., Champey, P., Gurgew, D., Ramsey, B., Singam, S. P., Speegle, C., and Thomas, N., "Achieving large-scale, high-resolution, full-shell replicated x-ray optics: budgeting for sources of angular-resolution errors," in [*Optics for EUV, X-Ray, and Gamma-Ray Astronomy XI*], O'Dell, S. L., Gaskin, J. A., Pareschi, G., and Spiga, D., eds., **12679**, 126791D, International Society for Optics and Photonics, SPIE (2023).

[5] Singam, S. P., Gaskin, J., Kolodziejczak, J., Speegle, C., Bongiorno, S., Baumgartner, W., Davis, J., Thomas, N., Champey, P., Gurgew, D., Davis, C., and Ramsey, B., "Recent advancements in full-shell x-ray optics at msfc," in [*AAS/High Energy Astrophysics Division Meeting*], **20**, 103.34, American Astronomical Society (September 2023). Conference poster.

[6] Ramsey, B. D., Alexander, C. D., Apple, J. A., Benson, C. M., Dietz, K. L., Elsner, R. F., Engelhaupt, D. E., Ghosh, K. K., Kolodziejczak, J. J., O'Dell, S. L., et al., "Hero: high-energy replicated optics for a hard-x-ray balloon payload," in [*X-Ray Optics, Instruments, and Missions III*], **4138**, 147–153, SPIE (2000).

[7] Baumgartner, W. H., Bongiorno, S. D., Gaskin, J. A., Gurgew, D. N., Ramsey, B. D., Singam, P., Smith, D. D., and Thomas, N. E., "High resolution full shell replicated x-ray optics for foxsi-4," *Space Telescopes and Instrumentation 2023: Ultraviolet to Gamma Ray* **12679**, 126790C, SPIE (2023).

[8] Krucker, S., Christe, S., Glesener, L., Ishikawa, S.-n., McBride, S., Glaser, D., and Turin, P., "First images from the focusing optics x-ray solar imager," *The Astrophysical Journal Letters* **793**(2), L32 (2014).

[9] Bongiorno, S. D., Baumgartner, W. H., Kolodziejczak, J., Davis, C. G., Ranganathan, J., Thomas, N., McCracken, J., and Gurgew, D., "Assembly of the FOXSI-4 mirror modules," in [*Optics for EUV, X-Ray, and Gamma-Ray Astronomy XI*], O'Dell, S. L., Gaskin, J. A., Pareschi, G., and Spiga, D., eds., **12679**, 126790D, International Society for Optics and Photonics, SPIE (2023).

[10] Ramsey, B. D., Alexander, C. D., Apple, J. A., Baumgartner, W. H., Bongiorno, S. D., Buz, J., Caldwell, A. D., Cash, J. L., Elsner, R. F., Gaskin, J. A., et al., "The imaging x-ray polarimetry explorer (ixpe): technical overview iv," *Space Telescopes and Instrumentation 2021: Ultraviolet to Gamma Ray* **11821**, 118210M (2021).

[11] Zhang, W. W., Allgood, K. D., Biskach, M. P., Chan, K.-W., Hlinka, M., Kearney, J. D., Mazzarella, J. R., McClelland, R. S., Numata, A., Riveros, R. E., et al., "High-resolution, lightweight, and low-cost x-ray optics for the lynx observatory," *Journal of Astronomical Telescopes, Instruments, and Systems* **5**(2), 021012 (2019).

[12] Harrison, F. A., Craig, W. W., Christensen, F. E., Hailey, C. J., Zhang, W. W., Boggs, S. E., Stern, D., Cook, W. R., Forster, K., Giommi, P., Grefenstette, B. W., Kim, Y., Kitaguchi, T., Koglin, J. E., Madsen, K. K., Mao, P. H., Miyasaka, H., Mori, K., Perri, M., Pivovaroff, M. J., Puccetti, S., Rana, V. R., Westergaard, N. J., Willis, J., and Zoglauer, A., "The nuclear spectroscopic telescope array (NuSTAR) high-energy x-ray mission," *The Astrophysical Journal* **770**, 103 (June 2013).

[13] Gaskin, J. A., Swartz, D. A., Vikhlinin, A., Özel, F., Gelmis, K. E., Arenberg, J. W., Bandler, S. R., Bautz, M. W., Betancourt-Martinez, G. L., Biskach, M. P., et al., "Lynx x-ray observatory: an overview," *Journal of Astronomical Telescopes, Instruments, and Systems* **5**(2), 021001 (2019).

[14] Singam, P., Speegle, C., Meekham, A., Kolodziejczak, J., Banks, D., Baumgartner, W., Gaskin, J., Bongiorno, S., Ramsey, B., Smith, D. D., et al., "Optimizing the electroforming process for full-shell x-ray optics," *Journal of Astronomical Telescopes, Instruments, and Systems* **10**(3), 034001 (2024).

[15] Singam, P., Speegle, C., Meekham, A., Kolodziejczak, J., Baumgartner, W., Davis, G., Banks, D., Gaskin, J., Bongiorno, S., and Ramsey, B., "Optimizing the electroforming process to enhance the thickness uniformity of full shell x-ray optics," in [*Optics for EUV, X-Ray, and Gamma-Ray Astronomy XI*], O'Dell, S. L., Gaskin, J. A., Pareschi, G., and Spiga, D., eds., **12679**, 126790B, International Society for Optics and Photonics, SPIE (2023).

[16] Gurgew, D. N. and Singam, S. P., "Characterization of nico multilayer coating stress for x-ray optic applications," *Space Telescopes and Instrumentation 2023: Ultraviolet to Gamma Ray* **12679**, 126790N, SPIE (2023).

[17] Chalifoux, B., Heilmann, R. K., and Schattenburg, M. L., "Simulations of film stress effects on mirror segments for the lynx x-ray observatory concept," *Journal of Astronomical Telescopes, Instruments, and Systems* **5**(2), 021004 (2019).